ELSEVIER

Journal of Alloys and Compounds 323–324 (2001) 260–266

Journal of ALLOYS AND COMPOUNDS

www.elsevier.com/locate/jallcom

Crystal field studies in Eu^{3+} doped $Bi_{12}SiO_{20}$ and $Bi_{12}SiO_{20}:V^{5+}$ single crystals

C. Cascales[a,*], P. Porcher[b], J. Fernández[c,d], A. Oleaga[c], R. Balda[c,d], E. Diéguez[e]

[a]*Instituto de Ciencia de Materiales de Madrid, CSIC, Cantoblanco, E-28049 Madrid, Spain*
[b]*Laboratoire de Chimie Appliquée de l'État Solide, UMR 7574-CNRS, ENSCP. 11 Rue Pierre et Marie Curie, F-75231 Paris, France*
[c]*Departamento de Física Aplicada I, Universidad del País Vasco, Alameda Urquijo s/n, E-48013 Bilbao, Spain*
[d]*Centro Mixto CSIC-UPV/EHU, Universidad del País Vasco, Alameda Urquijo s/n, E-48013 Bilbao, Spain*
[e]*Departamento de Física de Materiales C-IV, Universidad Autónoma de Madrid, E-28049 Madrid, Spain*

Abstract

Site-selective laser spectroscopy investigations of Eu^{3+} in $Bi_{12}SiO_{20}$ (BSO) and $Bi_{12}SiO_{20}:V^{5+}$ (BSO:V) single crystals have been carried out. The line narrowed fluorescence shows the existence of a single crystal field site for the rare earth in BSO whereas in BSO:V five different crystal field sites for Eu^{3+} may exist, which depend on the vanadium concentration. The number of Stark components observed in $^5D_0 \rightarrow {}^7F_J$ transitions corresponds to a complete absence of degeneracy in ^7F_J multiplets and indicates a symmetry C_{2v} or lower for these optically active centres. Simulations of the sequence of Eu^{3+} energy levels for each of the five observed sites have been worked out by using the single-particle crystal-field theory. The nature of the new active optical sites has also been investigated by comparing the phenomenological crystal-field parameters with those calculated by a semi-empirical model which takes into account the distortions of the oxygen bonds produced by the presence of V^{5+}. © 2001 Elsevier Science B.V. All rights reserved.

Keywords: Optical properties; Luminescence; Crystal structure and symmetry; Crystal and ligand field; Crystal growth

1. Introduction

A growing interest is focused on $Bi_{12}SiO_{20}$ (BSO) due to its optical properties and technological applications, most of them derived from its photorefractive behaviour [1].

Bismuth oxide compounds of the $Bi_{12}SiO_{20}$ type have a body-centered cubic structure (sillenite structure) which is able to accommodate a variety of different M atoms (M = Si in this compound). This is due to the fact that the oxygen tetrahedron surrounding the M atom can change its size without a major effect on the remaining atomic arrangement [2]. This peculiarity has promoted an effort to establish the mechanisms of isomorphous replacement in sillenites. From a fundamental point of view the knowledge of the defects responsible for the photorefractive effect still remains as an unsolved question, in particular as regards to the absorption bands associated with those defects. Up to now most of the works adscribe the absorption shoulder, located at energies close to the absorption edge, to the photoconductive and photorefractive behaviour. However, no definite conclusions have been reached about which defects are responsible for these behaviours.

BSO crystals doped with several transition metal ions have been studied [3–6] in order to ascertain their influence on the absorption shoulder appearing in pure BSO crystals. Among them, V^{5+} has shown very interesting features. In particular, it has been demonstrated [7] that at small concentrations V^{5+} gives an increase of the absorption coefficient in the shoulder region whereas at higher concentrations a bleaching of the BSO crystals occurs. Moreover, the presence of V^{5+} in the sillenite structure strongly affects the type of Bi–O bondings, and therefore, the Bi site symmetry [8,9]. On the other hand, only a few studies are known on the optical properties of BSO doped with rare earths [10–16]. It is well established that spectroscopical studies of rare earths may give valuable information about lattice site, lattice distortion, degree of covalency to ligand ions, and many other related dopant-host properties.

In recent works [14,15] some of the present authors reported, for the first time in pure and vanadium codoped BSO crystals, a preliminary identification of the spectro-

*Corresponding author. Tel.: +34-1-334-9027; fax: +34-1-372-0623.
E-mail address: ccascales@icmm.csic.es (C. Cascales).

0925-8388/01/$ – see front matter © 2001 Elsevier Science B.V. All rights reserved.
PII: S0925-8388(01)01026-X

scopic active sites of Nd^{3+} and Eu^{3+} ions by using site-selective laser spectroscopy. Three different crystal-field sites for Nd^{3+} and five different crystal-field sites for Eu^{3+}, which depend on vanadium concentration, were found and optically isolated. However, neither a clear explanation was found about the nature and characteristic features presented by the emission spectra corresponding to the optical active sites, nor a plausible argument permitting to relate the rare earth optical behaviour with the presence of vanadium in the BSO crystal structure.

The work reported here comprises the spectroscopic results on site-selective emission spectra and a detailed crystal-field (cf) simulation of the Eu^{3+} energy level scheme for the five different optical centres in the BSO host. Calculations of cf effects have been carried out by using the single-particle cf theory. The phenomenological simulation of each Eu^{3+} energy level scheme is conducted on the basis of the strongly reduced $^7F_{JM}$ set alone, i.e. only considering $49|SLJM_J\rangle$ levels. A descending symmetry method, from C_{2v} to C_2 symmetries, has been used in the fitting procedure. The appearance and relative intensity of these centres are discussed in terms of plausible crystallographic distortions of the EuO_5 polyhedron when compared with the BiO_5 in the non-substituted BSO host. Simulations of corresponding cf parameters for these changes in the Bi environment were performed through a semi-empirical model which considers the crystallographic positions of the oxygen atoms around Bi.

2. Experimental

Pure and doped BSO crystals were grown by the Czochralski method from grade A1 Johnson-Matthey powder. Several crystals were grown with rare earth concentrations up to 10 000 ppm in the melt. The absorption spectra of these samples revealed that a Eu^{3+} saturation is attained at concentrations greater than 5000 ppm. For this reason the codoped vanadium crystals (with vanadium contents of 100, 200, 500, and 999 ppm) were obtained while keeping 5000 ppm for rare earths.

The samples temperature was varied between 4.2 and 300 K with a continuous flow cryostat. Time-resolved fluorescence line-narrowed emission spectra of the $^5D_0 \rightarrow {}^7F_J$ transitions of Eu^{3+} were performed by exciting the samples with a pulsed tunable dye laser of 9 ns pulse width and 0.08 cm^{-1} linewidth. The fluorescence was analyzed and detected with a EGG-PAR optical multichannel analyzer.

3. Eu^{3+} spectroscopy

Time-resolved line-narrowed fluorescence spectra of the $^5D_0 \rightarrow {}^7F_J$ transitions of Eu^{3+} in singly doped and vanadium codoped crystals were obtained at 4.2 K by using different resonant excitation wavelengths into the $^7F_0 \rightarrow {}^5D_0$ transition. These spectra were obtained at different time delays after the laser pulse. As an example, Fig. 1a shows the $^5D_0 \rightarrow {}^7F_{0,1,2}$ spectra at 4.2 K for a BSO crystal doped with 5000 ppm of Eu^{3+} obtained at 1 ms after the laser pulse by exciting at 579.1 nm. As can be observed the spectrum shows the $^5D_0 \rightarrow {}^7F_0$ transition with a comparable intensity to the $^5D_0 \rightarrow {}^7F_1$ one. It shows three peaks in the $^5D_0 \rightarrow {}^7F_1$ region and five peaks for the $^5D_0 \rightarrow {}^7F_2$ transition. Thus, on the basis of the J splittings, we can assign the spectrum to sites of C_{2v} symmetry or lower. A systematic excitation performed along the $^7F_0 \rightarrow {}^5D_0$ transition did not reveal the existence of any other sites for Eu^{3+} ions in the BSO crystal.

Similar time-resolved line-narrowed emission spectra performed in vanadium codoped crystals show that in the samples codoped with small quantities of vanadium (100–

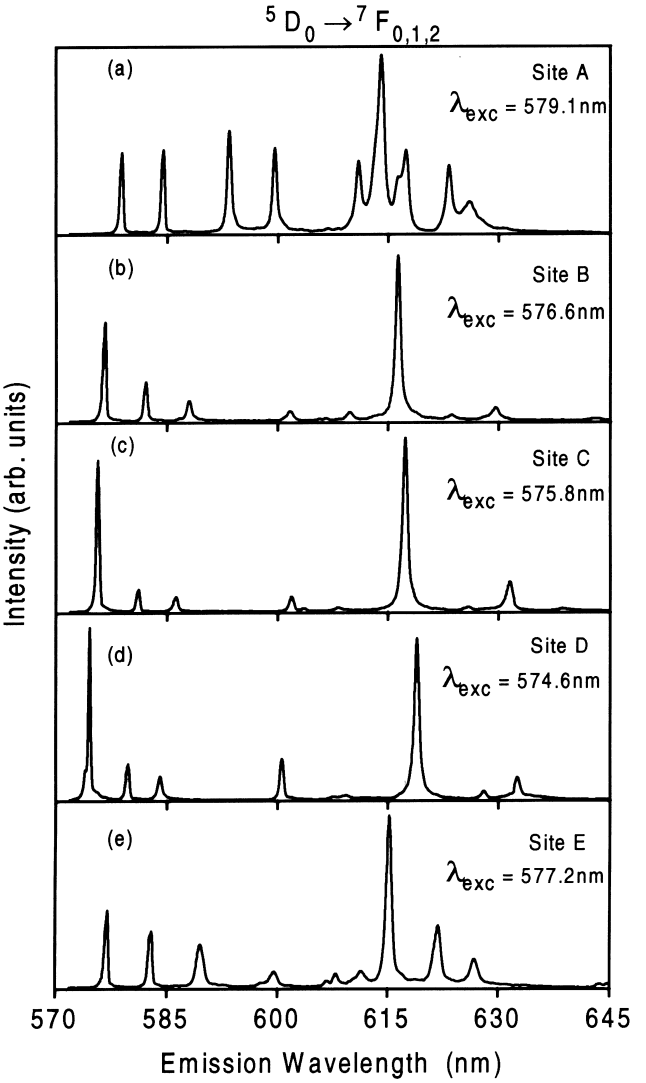

Fig. 1. Emission spectra of $^5D_0 \rightarrow {}^7F_{0,1,2}$ transitions at 4.2 K exciting at different wavelengths: (a) for BSO:Eu^{3+} = 5000 ppm; (b), (c), and (d) for BSO:Eu^{3+} = 5000 ppm, V^{5+} = 200 ppm; (e) for BSO:Eu^{3+} = 5000 ppm, V^{5+} = 999 ppm.

200 ppm) three new sites appear (sites B, C, and D) whereas the former site (labelled site A) decreases its intensity. The spectrum obtained by exciting at 579.1 nm is similar to that found in BSO singly doped crystal. On the contrary, the three new spectra obtained by exciting at 576.6, 575.8, and 574.6 nm, respectively, show different features as can be seen in Fig. 1b–d. These spectra were obtained for a sample codoped with 200 ppm of vanadium. The ratio of the $^5D_0 \rightarrow {}^7F_2$ and $^5D_0 \rightarrow {}^7F_1$ emission intensities reveals an enhancement of the electric-dipole transition due to an increasing distortion of the oxygen atoms polyhedron surrounding Eu^{3+} ions for these three new sites.

At vanadium concentrations around 500 ppm, site A vanishes, a new site named E appears, whereas sites B, C, and D remain the same. As an example Fig. 1e shows the spectrum at 4.2 K for a BSO crystal codoped with 5000 ppm of Eu^{3+} and 999 ppm of V^{5+} obtained at 1 ms after the laser pulse by exciting at 577.2 nm. The energy levels for sites B, C, and D are almost the same as for the sample with a low vanadium concentration.

The experimental energy levels for A, B, C, D and E sites in $Bi_{12}SiO_{20}$ and $Bi_{12}SiO_{20}$:V^{5+} are given in Table 1.

4. Structural considerations

The existence of several possible sites for rare earths in BSO can be understood on the basis of its structural framework. As shown in Fig. 2, the ideal sillenite structure is built up by Bi-polyhedra connected via common edges to form dimers that link translationally identical $[MO(3)_4]$ tetrahedra. Recent neutron diffraction studies [8,9] have shown the existence of sillenites with M cations having an effective valence lower than four and with a structure being to a great extent O(3) atom defective. This last property ensures the possibility for Bi^{3+} cations to occupy M sites where the missing vertex provides space for hosting the lone $6s^2$ electron pair. It has also been proved [8,9] that trivalent ions like Ga^{3+} and Fe^{3+} may occupy M sites having a regular tetrahedral environment. Moreover, ions with a valence greater than four, such as V^{5+} or P^{5+}, occupying M sites can give stable sillenites because Bi atoms, whose polyhedra build up the framework, can change not only the geometry of the coordination environments but also the coordination itself and provide a great structural flexibility.

The presence of trivalent and pentavalent cations in M sites changes the bond lengths in the above structures and induces changes in the geometry of Bi polyhedra as compared to Bi-polyhedra of an ideal sillenite. As a consequence, trivalent rare earth ions occupying Bi sites will experience different crystal field sites, and therefore they should exhibit site dependent optical properties. If we take into account that there are three of such polyhedra linked to each tetrahedron corner we could conclude that the first effect of V^{5+} on rare earth ions is to distort their environment and therefore to produce non-equivalent crystal field sites for the rare earth (B, C, D sites). Although an accurate estimation of the fraction of Eu^{3+} ions in different sites is difficult, we can approach this number by taking into account the excitation spectra of Eu^{3+}-doped BSO for B, C, and D sites, under the assumption that the absorption cross-sections are similar for these sites. The result has shown that the spectrum corresponding to site C is the most intense one among B, C, and D sites, the ratio among this spectrum and those corresponding to sites B and D being of the order of 31.9 for C/B and 24.17 for C/D. These values suggest that the occupation number for site C is at least one order of magnitude higher than those for sites B and D which are quite similar. At higher vanadium concentrations ($\geq$500 ppm) some new defects appear in the BSO structure due to the presence of O(4) atoms necessary to compensate the presence of V^{5+} ions in M sites [8,9]. These defects could further promote the appearance of new sites such as the observed E site.

In the next paragraph we shall discuss how the presence of V^{5+} ions occupying M sites can induce significant variations in the O(3)–Bi–O(1b) bond distances leading to the observed increase of the phenomenological cf parameters.

5. Crystal-field analysis and simulation of the energy level schemes

The phenomenological cf simulation of the Eu^{3+} energy level scheme can be conducted on the basis of the $^7F_{JM}$ set alone by using only 49 levels out of a total of 3003 of the $4f^6$ Eu^{3+} configuration. The use of this truncation is enabled by two facts: firstly, the cf operator mixes only the levels with the same multiplicity, and secondly, the ground ^7F_J ($J=0-6$) term is well isolated from the rest of the configuration (about 12 000 cm^{-1} between $^7F_6$ and $^5D_0$), which renders the mixing of the wavefunctions negligible. Thus, an accurate simulation of the cf effect is allowed by considering only this strongly reduced basis, i.e. $49|SLJM_J\rangle$ states [17,18].

The method used for calculating the energy levels of Eu^{3+} in its crystalline environment usually considers the single-particle cf theory [19,20]. Following Wybourne's formalism the cf hamiltonian is expressed as a sum of products of tensor operators $(C_q^k)_i$, with real B_q^k and complex S_q^k parameters as coefficients [19]:

$$H_{\mathrm{CF}} = \sum_{k=2}^{4,6} \sum_{q=0}^{k} \left[B_q^k (C_q^k + (-1)^q C_{-q}^k) + i S_q^k (C_q^k - (-1)^q C_{-q}^k) \right] \quad (1)$$

The number of non-zero B_q^k and S_q^k phenomenological cf

Table 1
Observed and calculated energy levels (cm^{-1}) for A, B, C, D, and E sites in BSO:Eu^{3+}

Level	Site A		Site B		Site C		Site D		Site E	
$^{2S+1}L_J$	Exp	Cal	Exp	Cal	Exp	Cal	Exp	Cal	Exp	Cal
$^7F_0$	0	0.1	0.1	0.2	0.1	0.2	0.1	0.2	0.1	0.1
$^7F_1$	163.4	166.7	168.2	158.5	161.7	157.7	156.8	146.2	177.9	177.3
	421.1	424.4	338.3	345.4	310.0	313.6	285.0	287.5	365.7	368.7
	594.7	587.7	727.1	730.1	755.0	754.2	755.1	763.2	651.3	648.3
$^7F_2$	906.1	898.7	1118.0	1111.2	929.2	916.3	–	978.4	883.1	892.3
	989.2	988.7	–	1165.4	–	1028.7	–	1027.2	973.0	976.4
	1042.4	1047.6	1306.6	1312.0	1170.4	1179.7	1243.9	1251.1	1072.9	1080.9
	1077.6	1084.4	1457.0	1459.3	1388.2	1392.2	1475.1	1472.2	1246.2	1229.4
	1228.8	1223.8	–	1600.3	1527.4	1523.8	1594.1	1597.2	1374.2	1366.3
$^7F_3$	–	1895.7	–	1826.6	–	1841.3	2148.8	1958.0	1797.3	1799.3
	–	1931.1	–	1858.5	–	1846.9	2204.8	1963.5	1823.3	1822.1
	1941.7	1937.7	2008.2	2006.9	–	2032.0	2305.1	2153.4	–	1921.7
	1994.6	1992.1	2063.7	2058.0	2126.2	2122.1	2337.8	2198.2	2010.1	2000.8
	2092.5	2096.9	2121.6	2121.7	2154.4	2156.3	–	2307.2	–	2071.8
	2139.0	2141.3	2157.7	2167.9	2227.7	2230.5	–	2337.7	2078.8	2075.9
	–	2234.4	2235.9	2233.5	2309.4	2311.2	–	2355.3	–	2180.1
$^7F_4$	–	2739.2	2872.6	2862.6	2838.9	2832.8	2894.2	2894.3	–	2569.8
	2825.9	2824.3	2909.4	2905.8	2931.9	2927.5	2952.4	2952.3	2750.9	2755.0
	2854.3	2845.6	2960.2	2965.6	2996.7	2996.7	–	2975.5	2851.5	2841.5
	2968.0	2970.0	3058.2	3051.1	–	3064.0	3024.3	3026.7	2863.3	2866.0
	3016.7	3009.8	3114.8	3113.0	3110.8	3112.2	3149.8	3142.9	2963.4	2965.1
	3077.6	3067.4	3152.7	3149.7	3168.3	3172.3	3209.5	3192.5	3046.0	3040.8
	3124.4	3125.4	–	3203.8	3224.2	3228.0	3290.1	3300.6	3095.6	3094.3
	3160.7	3164.2	3214.2	3226.0	3265.0	3267.0	3306.0	3310.5	3160.7	3169.0
	3194.6	3199.3	3261.7	3270.1	3302.2	3302.2	3335.2	3342.8	–	3248.0
$^7F_5$	3772.7	3769.3	3717.6	3725.0	3754.3	3768.8	3773.0	3797.1	–	3715.8
	–	3798.0	3753.2	3754.6	3790.4	3790.2	3838.7	3824.7	3722.6	3719.5
	3855.4	3857.8	3930.0	3932.5	3971.8	3969.7	4008.4	4004.0	3870.2	3882.0
	3897.4	3894.0	–	3988.0	4029.5	4035.4	4023.6	4022.7	–	3935.0
	3987.5	3987.0	4012.6	4010.6	4100.5	4093.3	4124.1	4120.9	3949.3	3949.6
	–	4070.4	4073.7	4072.7	4158.1	4152.0	4168.9	4178.6	–	3996.8
	4088.0	4091.4	4220.2	4222.4	4222.9	4226.1	4269.6	4258.5	4047.0	4047.0
	–	4100.5	–	4251.8	4269.9	4271.1	4313.5	4314.4	4114.3	4100.2
	–	4181.7	–	4256.7	–	4295.6	4354.4	4367.8	4172.3	4172.3
	–	4208.2	–	4340.2	–	4445.7	–	4485.9	4353.6	4361.8
	–	4237.2	4381.4	4373.7	4470.4	4459.9	4580.5	4572.1	–	4364.0
$^7F_6$	–	4649.9	4691.2	4701.8	4715.9	4730.8	4747.1	4752.4	(4688.4)	4688.4
	4654.0	4654.9	4717.3	4710.8	4766.6	4750.3	–	4817.3	–	4688.7
	4950.7	4961.1	–	4906.9	–	4975.9	4842.3	4840.0	–	5042.6
	–	4962.5	-	4943.4	5000.7	4998.7	–	4948.5	–	5087.9
	–	5053.8	5009.0	5009.6	–	5105.8	5033.6	5051.4	–	5122.8
	–	5067.0	–	5069.0	–	5140.3	5166.4	5144.2	–	5138.9
	–	5082.1	–	5306.2	–	5442.5	5370.1	5365.5	–	5162.0
	–	5147.9	–	5414.5	–	5531.0	–	5489.9	–	5266.6
	5169.0	5161.7	–	5478.3	–	5598.5	–	5548.3	–	5272.2
	–	5277.5	–	5675.5	–	5782.4	–	5749.7	–	5481.9
	–	5285.6	–	5678.9	–	5784.9	–	5752.4	–	5484.1
	–	5426.6	–	5909.2	–	6009.7	–	5983.5	–	5737.5
	–	5426.8	–	5910.5	–	6010.4	–	5983.8	–	5737.6

parameters depends on the crystallographic point-site symmetry of the lanthanide ion in the considered host. In the special case of the C_2 (C_s) symmetry for the different Eu^{3+} active centres in the BSO matrix, the cf Hamiltonian comprises as much as 15 parameters including six imaginary ones, although one of them, S_2^2, can be cancelled by an appropriate choice of the reference axis system. Accordingly, in order to make the simulation carefully, we carry

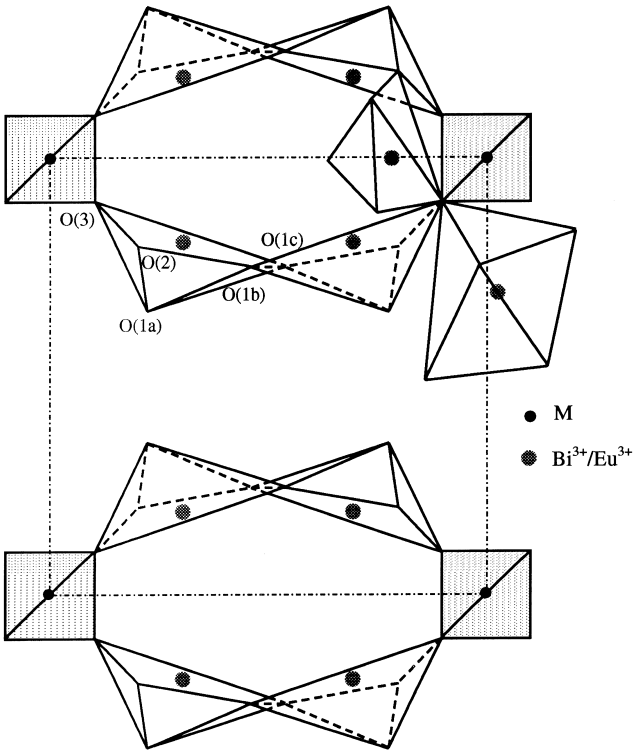

Fig. 2. Fragment of the sillenite structure $Bi_{12}MO_{20}$.

out a descending symmetry procedure, from C_{2v} (nine real B_q^k parameters) to C_2 (C_s) symmetries, in which second, fourth, and sixth-rank cf parameters were carefully determined from the adequate reproduction of $^7F_1$, $^7F_2$, and the remaining observed ^7F_J splittings, respectively, before considering all observed energy levels and a free variation of all cf parameters.

The laborious procedure of obtaining the cf parameters will be strongly facilitated if their starting values could be estimated by a semi-empirical calculation model from crystallographic positions. For this reason and in order to compare with phenomenological values, the so-called simple overlap model (SOM) [21,22] was now applied. In SOM it is assumed that the interaction energy of the rare earth R^{3+} in a crystalline environment is produced by an electrostatic potential created by charges which are uniformly distributed over small regions centered around the mid-point of the R_L distance from R^{3+} to the ligand L, R_0 being the shortest distance. The charge in each region is proportional to the total overlap integral ρ between the 4f and the s and p orbitals of R^{3+} and L, respectively. The cf parameters are written as

$$B_q^k = \langle r^k \rangle \sum_L \rho_L \left(\frac{2}{1 \pm \rho_L} \right)^{k+1} A_q^k(L) \quad \rho = \rho_0 \left(\frac{R_0}{R_L} \right)^{3.5} \qquad (2)$$

The sum runs over all ligands of the first coordination sphere, and consequently required crystallographic data restricted to the closest L positions, and $\langle r^k \rangle$ radial integrals [23] are not corrected from the spatial expansion. The overlap degree ρ in the wavefunctions associated to the bonding between the metal and L varies for each ligand as a function of the distance from the central ion and is referred to the closest ligand. A_q^k is the lattice sum and it takes into account the symmetry properties of the metal site, including the effective charge attributed to the ligand. The sign $\pm$ of the denominator stands for the following: when a single type of ligand is considered, a sign – corresponding to the normal shift of the charge barycenter from the middle of the bonding distance should be taken, and when different ligands are present the sign – corresponds to the most covalent one.

Comparisons between experimental and semi empirical SOM cf parameters were made through the corresponding crystal field strengths S_k, for the cf parameters of rank k, and the total crystal field strength, S_T, [24]. In these comparisons the two adjustable parameters required for the model were fixed to the typical values of -0.8 for the effective charge for the oxygen [25], and 0.05, 0.06, 0.07, and 0.08 for the overlap ρ [26,27]. Crystallographic data were taken from Ref. [28].

The actual fitting of the experimental data, schemes of 30, 30, 32, 36, and 29 energy levels for A, B, C, D, and E sites, respectively, was conducted with the aid of the matrix diagonalizing program GROMINET [29], which took into account the J mixing between wavefunctions with different J and M values.

6. Discussion

The five energy level schemes for each of the optically active sites are characterized by strong splittings of the $^7F_{1-6}$ levels under the cf effect, and in accordance very large cf parameters can be expected to be obtained. The close resemblance of these schemes from B, C, and D active sites in BSO is evidently due to the rather similar coordination of the Eu^{3+} in each case. From this point of view, differences observed in optical spectra corresponding to the two remaining A and E sites clearly suggest different crystallographic environments.

Phenomenological calculations carried out with C_{2v} and then C_2 (C_s) point symmetries yielded energy level schemes in very good agreement with the experimental data, as can be seen in Table 1, and in addition to the low overall σ values obtained with each of the five cf parameter sets (Table 2), no significant individual discrepancies occur between the calculated and experimental energy levels. The less satisfactory figure of merit, 11.8 cm^{-1}, for the simulation of the D site, is mostly due to the discrepancy found only for two levels, 3773.0 and 5166.4 cm^{-1}, which in fact descends to a similar value, 8.7 cm^{-1}, if they are not considered.

When A, B, C, and D sites are compared, the progressive increase of phenomenological crystal field strengths S_k

Table 2
Crystal field parameters for different observed A, B, C, D, and E sites in BSO:Eu^{3+} [a]

	Site A	Site B	Site C	Site D	Site E
B20	85(19)	−367(14)	−470(14)	−576(20)	−157(19)
B22	888(12)	1404(9)	1433(10)	1472(14)	1034(16)
B40	234(39)	848(40)	1545(37)	892(42)	835(52)
B42	600(24)	42(28)	172(27)	−43(30)	272(44)
S42	−234(43)	−292(62)	400(45)	1249(29)	−305(35)
B44	174(24)	−550(25)	−486(29)	−442(35)	−185(56)
S44	271(39)	494(41)	−868(40)	−715(32)	1585(25)
B60	1205(40)	−800(40)	−945(40)	−460(45)	1050(48)
B62	−1041(27)	−917(25)	−604(31)	−1011(31)	−454(44)
S62	226(51)	11(64)	−192(47)	97(37)	136(41)
B64	−163(48)	139(34)	59(40)	−556(41)	−307(48)
S64	330(40)	−354(55)	203(36)	502(46)	−32(53)
B66	−356(28)	−173(31)	−353(40)	−57(49)	764(37)
S66	−136(74)	17(38)	−273(39)	−36(34)	−364(42)
σ [b]	7.9	7.5	8.7	11.8	9.8
Levels	30	30	32	36	29
Residue	1002	908	1369	3048	1338
S_2	563	903	930	966	658
S_4	348	470	726	770	826
S_6	574	453	410	512	473
S_T	506	643	721	772	668

[a] Values in parentheses are the estimated standard deviations. Units in cm^{-1}.
[b] $\sigma = [\Sigma(E_{exp} - E_{cal})^2/(N_{lev} - N_{par})]^{1/2}$. Where E_{exp} and E_{cal} are the experimental and calculated energy level values and N_{lev} and N_{par} are the number of levels and parameters, respectively.

is observed. It would indicate that the deviation from the C_2 (C_s) site symmetry for the Eu^{3+} environment is getting more important, i.e. although the nature of the (Bi, Eu)O_5 polyhedra is the same, it become more distorted. Noteworthy differences are found for site E. It assumes smaller splitting values of the $^7F_1$ level, and consequently more reduced second order parameters.

Table 3 lists the phenomenological along with semi-empirical SOM calculated crystal-field strengths, S_k, for each observed Eu^{3+} site, which in each case, depend on the considered ρ overlap. SOM seems to be able to reproduce the phenomenological cf strengths when local distortions around Bi^{3+} are supposed. Benefiting from the fact that SOM uses the crystallographic positions of BiO_5 coordination polyhedra in the estimation of the set of cf parameters, attempts of evaluating the possible distortion of this polyhedron were performed. For this purpose, systematic shifts between −8 and +8% with respect to the previously determined [28] positions of all oxygens, O1, O2, and O3, involved in the first coordination sphere of Bi^{3+}, were introduced. Values of the ρ overlap were maintained in the 0.05 – 0.08 range. In Table 3 we show

Table 3
Phenomenological and SOM simulated cf S_k strengths for selected distortions[a] of the Eu^{3+} environment in the BSO host[b]

Simulated	$\rho = 0.06$							
	Eu–O1a(Å)	Eu–O1b (Å)	Eu–O1c (Å)	Eu–O3 (Å)	S_2	S_4	S_6	S_T
NSS[c]	2.0637	2.2225	2.6217	2.6466	203	565	344	400
−5%O1, −5%O3	2.1376	1.9552	2.7432	2.4149	586	673	529	599
−6%O1, −6%O3	2.1570	1.9035	2.7704	2.3975	700	694	638	678
−7%O1, −7%O3	2.1770	1.8500	2.7984	2.3904	813	735	783	778
Phenomenological								
Site A	–	–	–	–	563	348	574	506
Site B	–	–	–	–	903	470	453	643
Site C	–	–	–	–	930	726	410	721
Site D	–	–	–	–	966	770	512	772
Site E	–	–	–	–	658	826	470	668

[a] Eu–O2 distance was held constant (2.2007 Å).
[b] $S_k = \{1/(2k+1)[(B_0^k)^2 + 2\Sigma_q[(B_q^k)^2 + (S_q^k)^2]]\}^{1/2}$ $S_T = \left[\frac{1}{3}\Sigma_k S_k^2\right]^{1/2}$.
[c] NSS non substituted sillenite.

for comparison the phenomenological cf strength parameters of the five different Eu^{3+} cf sites and the simulated values for an overlap of $\rho = 0.06$ and three different shifts of the O(1) and O(3) positions: −5, −6, and −7%. As can be seen, these distortions produce a noticeable shortening of the Eu–O(3) and Eu–O(1b) distances and a small increase of the Eu–O(1a) and Eu–O(1c) distances. The obtained results suggest that the presence of V^{5+} occupying M sites shortens $O^{M}(3)$–Bi^{3+}(RE) and Bi^{3+}(RE)–O(1b) distances and allows the increase of the S_2 cf parameter of the RE which replaces these bismuth atoms. This distortion also influences the Bi^{3+} sites of the nearby polyhedron of the dimer unit constituting the sillenite structure, and gives rise to the different observed cf sites. The shortening of the $O^{M}(3)$–Bi^{3+}(RE) distances in the vanadium doped sillenite is produced by the higher radius (59 pm) of the V^{5+} ion if compared with Si^{4+} (26 pm) and has been observed in sillenites with statistical distributions of M cations M = (Bi, V) [9]. The displacement of the O(3) atoms along the triad symmetry axis does not lead to an excessive local stress in the structure due to its relaxation capacity based on the flexible geometry of the Bi polyhedra.

It is worthy to notice that the distortion induced in the oxygen bonds by the different size of the V^{5+} ion is not the only mechanism responsible for the observed spectroscopic properties. Other mechanisms mentioned above such as charge compensation effects and/or oxygen vacancies could also play an important role and should not be disregarded.

7. Conclusions

On the basis of the above arguments and account taken of the great flexibility of the BSO structure, the difficulty to assign particular sites to a rare earth in the BSO structure becomes clear. Nevertheless, regarding the spectroscopic results of Eu^{3+} ions in BSO it is worthwhile noticing the extreme sensitivity of the Bi polyhedra geometry to the presence of V^{5+} ions. Moreover, these geometrical changes are very sharply defined, and as the Eu^{3+} spectroscopy shows, they do not seem to present a random nature which would give very wide inhomogeneous broadened emission lines. From these results it is well established that sites B, C, and D appear at very low V^{5+} concentrations and that their spectral characteristics remain unchanged up to the highest concentrations studied around 1000 ppm. On the other hand, the cf simulations performed by taking into account possible oxygen–RE bond length changes due to the presence of V^{5+} in M sites, suggest that the increase of S_k parameters is related to the decrease of $O^{M}(3)$–Eu^{3+} and Eu^{3+}–O(1b) distances and predict, as observed, a progressive increase of phenomenological crystal field strengths, S_k, for A, B, C, and D sites.

Acknowledgements

This work has been financially supported by the Spanish Government CICYT (Ref. MAT97-1009) and Basque Country University (ref: G21/98).

References

[1] L. Arizmendi, J.M. Cabrera, F. Agulló-López, Int. J. Optoelectron. 7 (1992) 149.
[2] S.C. Abrahams, J.L. Bernstein, C. Svensson, J. Chem. Phys. 71 (1979) 788.
[3] W. Wardzynski, H. Szymczak, J. Phys. Chem. Sol. 45 (1984) 887.
[4] T.V. Panchenko, N.A. Truseyeva, Ferroelectrics 115 (1991) 73.
[5] V.M. Orlov, M.V. Shilova, E.E. Kolosov, Izv. Akad. Nauk. SSSR, Neorg. Mater. 22 (1986) 507.
[6] Y. Nagao, Y. Mimura, Mater. Res. Bull. 24 (1989) 239.
[7] D. Nesheva, Z. Aneva, Z. Levi, J. Phys. Chem. Solids 56 (1995) 241.
[8] S.F. Radaev, V.I. Simonov, Yu.F. Kargin, V.M. Skorikov, Eur. J. Solid State Inorg. Chem. 29 (1992) 383.
[9] S.F. Radaev, V.I. Simonov, Sov. Phys. Cryst. 37 (1992) 484.
[10] A.D. Bondarev, E.I. Leonov, A.V. Nyavro, V.A. Chaldyshev, Opt. Spectrosc. (USSR) 56 (1984) 518.
[11] V.A. Belyaev, Yu.F. Biryulin, A.D. Bondarev, E.I. Leonov, O.A. Lupal, Yu.V. Shmartsev, Sov. Tech. Phys. Lett. 4 (1978) 478.
[12] T. Katsumata, K. Hanamori, Y. Akiyama, Y. Nobe, Mat. Res. Bull. 30 (1995) 19.
[13] G.A. Ambrazyavichyus, G.A. Babonas, A.D. Bondarev, E.I. Leonov, Opt. Spectrosc. 51 (1981) 99.
[14] A. Oleaga, R. Balda, J. Fernández, M.D. Serrano, E. Diéguez, J. Lumin. 71 (1997) 305.
[15] J. Fernández, A. Oleaga, R. Balda, M.D. Serrano, E. Diéguez, M.A. Arriandiaga, Opt. Mater. 8 (1997) 91.
[16] F. Ramos, D. Jaque, J. Romero, J. García Solé, U. Caldiño, J. Phys. Condens. Matter 11 (1999) 3201.
[17] C. Cascales, E. Antic Fidancev, M. Lemaitre Blaise, P. Porcher, J. Sol. State Chem. 89 (1990) 118.
[18] C. Cascales, E. Antic Fidancev, M. Lemaitre Blaise, P. Porcher, J. Alloys Comp. 180 (1992) 111.
[19] B.G. Wybourne, Spectroscopic Properties of Rare Earths, Wiley, New York, 1965.
[20] S. Hüfner, Optical Spectra of Transparent Rare Earth Compounds, Academic Press, New York, 1978.
[21] O.L. Malta, Chem. Phys. Lett. 88 (1982) 353.
[22] P. Porcher, M. Couto dos Santos, O. Malta, Phys. Chem. Chem. Phys. 1 (1999) 397.
[23] A.J. Freeman, J.P. Desclaux, J. Magn. Magn. Mat. 12 (1979) 11.
[24] N.C. Chang, J.B. Gruber, P.R. Leavitt, C.A. Morrison, J. Chem. Phys. 76 (1982) 3877.
[25] C.A. Morrison, R.P. Leavitt, Spectroscopic properties of triply ionized lanthanides in transparent host crystals, in: K.A. Gschneidner Jr, L. Eyring (Eds.), Handbook On the Physics and Chemistry of Rare Earths, Vol. 5, North Holland, Amsterdam, 1996.
[26] J.D. Axe, G. Burns, Phys. Rev. 152 (1966) 331.
[27] D. Garcia, M. Faucher, J. Chem. Phys. 82 (1985) 5554.
[28] S.F. Radaev, L.A. Muradyan, V.A. Sarin, V.N. Kanepit, A.N. Yudin, A.A. Mar'in, V.I. Simonov, Dokl. Akad. Nauk SSSR 307 (1989) 606.
[29] P. Porcher, Fortran routine GROMINET for simulation of real and complex crystal field parameters on $4f^{6}$ and $4f^{8}$ configurations, (1995) unpublished.